Spread of infectious diseases in a hyperbolic reaction-diffusion susceptible-infected-removed model

Elvira Barbera, Giancarlo Consolo, and Giovanna Valenti
Department of Mathematics and Computer Science, University of Messina, V. le F. D'Alcontres 31, I-98166 Messina, Italy
(Received 29 May 2013; revised manuscript received 2 August 2013; published 25 November 2013)

A one-dimensional hyperbolic reaction-diffusion model of epidemics is developed to describe the dynamics of diseases spread occurring in an environment where three kinds of individuals mutually interact: the susceptibles, the infectives, and the removed. It is assumed that the disease is transmitted from the infected population to the susceptible one according to a nonlinear convex incidence rate. The model, based upon the framework of extended thermodynamics, removes the unphysical feature of instantaneous diffusive effects, which is typical of parabolic models. Linear stability analyses are performed to study the nature of the equilibrium states against uniform and nonuniform perturbations. Emphasis is given to the occurrence of Hopf and Turing bifurcations, which break the temporal and the spatial symmetry of the system, respectively. The existence of traveling wave solutions connecting two steady states is also discussed. The governing equations are also integrated numerically to validate the analytical results and to characterize the spatiotemporal evolution of diseases.

DOI: 10.1103/PhysRevE.88.052719 PACS number(s): 87.23.Cc, 89.75.Hc, 87.19.X−, 05.45.−a

I. INTRODUCTION

Nowadays infectious diseases are still the major causes of mortality in developing countries, so that the possibility of predicting their spread is a compelling challenge in many fields, such as public health, agriculture, and zoology. For this reason, the proper characterization of the temporal evolution of the population becomes fundamental for the understanding of the underlying dynamics and for the definition of the mathematical model which better reproduces the scenario under investigation. In particular, many efforts have been devoted to the development of epidemiological models based on different mathematical approaches, either deterministic or stochastic [1–6]. Furthermore, with the aim of describing the spread of epidemics in a more realistic way, several spatially extended models, mostly based on systems of parabolic reaction-diffusion equations, have been also proposed [7–13]. However, the parabolic character of these models would lead the disease to propagate instantaneously over large distances. This unphysical feature can be overcome by building up a hyperbolic system [14,15]. Indeed, such a kind of system has been successfully applied in many different contexts like forest fire models [16], chemical and ecological systems [17–21], population dynamics [22,23], spread of hantavirus infection [24], transmission lines, and nonlinear oscillators [25].

Therefore, in this paper we make use of the theoretical framework of the extended thermodynamics [26] to develop a hyperbolic reaction-diffusion model describing the spatiotemporal interactions among susceptible, infected, and removed individuals. In our model the disease is assumed to be transmitted from the infected population to the susceptible one through a nonlinear convex incidence rate.

The paper is organized as follows. In Sec. II we build up the one-dimensional hyperbolic reaction-diffusion model of epidemics governing the above-mentioned population dynamics. In Sec. III we perform a linear stability analysis on the steady states. In particular, we investigate their stability against homogeneous and nonhomogeneous perturbations and focus our attention on the occurrence of Hopf and Turing bifurcations. As is known, the space-independent Hopf bifurcation breaks the temporal symmetry of a system and gives rise to oscillations that are uniform in space and periodic in time. On the other hand, the diffusion-driven Turing instability breaks the spatial symmetry and manifests itself through the formation of "patterns" that are stationary in time and oscillatory in space [27]. The analytical results here obtained are then compared, in Sec. IV, to the ones arising from the numerical integration of the governing equations.

Another approach for investigating the spatial spread of infection involves the analysis of traveling wave solutions. In particular, within the theoretical framework of wave propagation in continuous media, the validation of an evolution model requires a qualitative response in terms of wave processes, which are expected to occur at finite velocity. This is in contrast to the scenarios encountered in parabolic models where the speed parameter is not subjected to any upper limit. Therefore, it is of a certain interest to characterize the behavior of the resulting traveling wave solutions admitted by the hyperbolic model herein proposed. Such an analysis is carried out, both analytically and numerically, in Sec. V. Finally, concluding remarks are made in Sec. VI.

II. HYPERBOLIC MODEL

We consider a one-dimensional epidemic model where the whole population is subdivided into three classes of individuals: the susceptibles, who can catch the disease; the infectives, who have already contracted the disease and can transmit it; and the removed, who are either recovered and immune or isolated. The dynamics of these species can be described through the following system of partial differential equations written in convenient dimensionless units:

$$\frac{\partial S}{\partial t} + \frac{\partial J^S}{\partial x} = A(1-S) - \beta S I^2, \tag{1}$$

$$\frac{\partial I}{\partial t} + \frac{\partial J^I}{\partial x} = \beta S I^2 - (A+\mu) I, \tag{2}$$

$$\frac{\partial R}{\partial t} + \frac{\partial J^R}{\partial x} = \mu I - A R, \tag{3}$$

*gconsolo@unime.it

where $S(t,x)$, $I(t,x)$, and $R(t,x)$ represent, respectively, the susceptibles, infectives, and removed, at time t and position x, measured with respect to some reference populations. Moreover A is the birth (death) rate of the population, μ is the recovery rate, and the transmission of the infection is governed by a nonlinear incidence rate βSI^2, with the parameter β representing the transmission rate.

From the biological point of view, according to our definition of S and I, we are thus assuming that the number of individuals locally is changing in time and that a susceptible will contact an infected with a rate proportional to the number of infecteds around. In particular, an incidence rate which increases more than linearly with respect to the number of infectives I takes places if an effective cooperativity exists among the infectives [28–35]. For example, it can be observed in vectored diseases where multiple exposures to the disease vector are necessary before infection occurs or if individuals could harbor low-level infections that did not make them infectious but did increase susceptibility. Such a nonlinear incidence rate gives rise to a convex function with respect to the numbers of infectives, which implies that, with the growth of the infective population, the probability for a single infective individual to pass the infection further increases [36,37]. From the mathematical point of view, such a choice also allows us to deal with a richer variety of dynamical behaviors with respect to the bilinear case βSI [28,29].

It should be noticed that, since the first two equations of system (1)–(3) are independent of the last one, we can hereafter focus our attention on the dynamics of susceptibles and infected only described by the subsystem (1) and (2).

Usually, according to Fick's law, the diffusion fluxes, J^S and J^I, are assumed to be proportional to the gradient of the corresponding densities, namely,

$$J^S = -D_S \frac{\partial S}{\partial x}, \quad J^I = -D_I \frac{\partial I}{\partial x}, \tag{4}$$

where the diffusion coefficients, D_S and D_I, take into account the diffusive transport mechanism of the susceptible and infected, respectively. Typically, in biological systems, the population of infected individuals (which play the role of process activators) are less mobile than healthy individuals (which act as process inhibitors), so that the relation $D_S > D_I$ holds.

In passing we note that the governing equations (1) and (2), together with the constitutive relations (4), coincide with the model proposed in Ref. [13] when only one spatial dimension is taken into account. Furthermore, for $\beta = 1$ the system under investigation reduces to the classical Gray-Scott model [38], which, in spite of being usually encountered in the context of kinetics of chemical species [7,39,40], has been also used to characterize the spread of epidemics [8,13,28,29].

It should be also emphasized that Fickian diffusion (4), inserted into the governing equations (1) and (2), leads to a parabolic reaction-diffusion system which, as known, admits instantaneous diffusive effects. This unphysical feature can be removed by making use of hyperbolic models. For this reason, following the guidelines of the extended thermodynamics theory [26], we develop a hyperbolic reaction-diffusion model to describe the finite velocity spread of infectious diseases.

To this aim, instead of assuming Fick's laws (4) as constitutive equations for the dissipative fluxes, we consider J^S and J^I to be field variables (as well as S and I) satisfying the following balance equations:

$$\begin{aligned} \frac{\partial J^S}{\partial t} + \frac{\partial T^S}{\partial x} &= G^S, \\ \frac{\partial J^I}{\partial t} + \frac{\partial T^I}{\partial x} &= G^I, \end{aligned} \tag{5}$$

where the constitutive functions, T^S, T^I, G^S, and G^I, must be determined in terms of the whole set of the independent variables constituting the field $\mathbf{E} = (S, I, J^S, J^I)$. Since we are interested in a process not far away from the thermodynamical equilibrium characterized by vanishing fluxes J^S and J^I, we suppose a linear dependence of the constitutive functions on the fluxes, that is,

$$\begin{aligned} T^S &= \nu(S,I) + \nu_1(S,I)J^S + \nu_2(S,I)J^I, \\ T^I &= \eta(S,I) + \eta_1(S,I)J^S + \eta_2(S,I)J^I, \\ G^S &= \gamma(S,I) + \gamma_1(S,I)J^S + \gamma_2(S,I)J^I, \\ G^I &= \delta(S,I) + \delta_1(S,I)J^S + \delta_2(S,I)J^I. \end{aligned} \tag{6}$$

Then, assuming that the balance equations (5) reduce to (4) in the stationary case, we easily deduce

$$\begin{aligned} T^S &= \nu(S), \quad G^S = -\frac{\nu'(S)}{D_S} J^S, \\ T^I &= \eta(I), \quad G^I = -\frac{\eta'(I)}{D_I} J^I, \end{aligned} \tag{7}$$

where the prime stands for the derivative of a given function with respect to its argument.

A further restriction on the constitutive functions (7) follows from the entropy principle. It assumes the existence of a concave entropy density h and an entropy flux ϕ, both depending on $\mathbf{E}$, and satisfying, for all solutions of system (1), (2), (5), and (7), the well-known entropy inequality

$$\frac{\partial h}{\partial t} + \frac{\partial \phi}{\partial x} \geqslant 0. \tag{8}$$

The compatibility of system (1), (2), (5), and (7) with (8) can be achieved through the use of the so-called Lagrange multipliers Λ, Γ, ξ, Ξ, as shown in Refs. [26,41], which must also be determined in terms of the whole set of the field variables. Then the searched compatibility leads to the following expressions for the entropy functions:

$$\begin{aligned} h &= \tilde{h}_0(S) + \hat{h}_0(I) + \frac{X(S)}{2} J^S J^S + \frac{Y(I)}{2} J^I J^I, \\ \phi &= \Lambda_0(S) J^S + \Gamma_0(I) J^I, \end{aligned} \tag{9}$$

while the Lagrange multipliers take the form

$$\begin{aligned} \xi &= X(S) J^S, \quad \Xi = Y(I) J^I, \\ \Lambda &= \Lambda_0(S) + \frac{X'(S)}{2} J^S J^S, \\ \Gamma &= \Gamma_0(I) + \frac{Y'(I)}{2} J^I J^I, \end{aligned} \tag{10}$$

where

$$\begin{aligned} \Lambda_0'(S) &= \nu'(S)X(S), \quad \Gamma_0'(I) = \eta'(I)Y(I), \\ \tilde{h}_0'(S) &= \Lambda_0(S), \quad \hat{h}_0'(I) = \Gamma_0(I). \end{aligned} \tag{11}$$

Finally, the concavity condition for h with respect to the field variables yields the further restrictions:

$$X(S) < 0,\ Y(I) < 0, \tag{12}$$

$$\nu'(S) > 0,\ \eta'(I) > 0. \tag{13}$$

As a consequence, the resulting system, which is obtained by considering (1) and (2) and substituting (7) into (5),

$$\begin{aligned}
&\frac{\partial S}{\partial t} + \frac{\partial J^S}{\partial x} = A(1-S) - \beta S I^2,\\
&\frac{\partial I}{\partial t} + \frac{\partial J^I}{\partial x} = \beta S I^2 - (A+\mu) I,\\
&\frac{\partial J^S}{\partial t} + \nu' \frac{\partial S}{\partial x} = -\frac{\nu'}{D_S} J^S,\\
&\frac{\partial J^I}{\partial t} + \eta' \frac{\partial I}{\partial x} = -\frac{\eta'}{D_I} J^I,
\end{aligned} \tag{14}$$

becomes symmetric hyperbolic in the sense of Friedrichs-Lax [42], and so the Cauchy problem is well posed for suitable smooth initial data [26]. Moreover, the concavity conditions (13) ensure that the characteristic velocities associated to the system (14),

$$\lambda_{1,2} = \pm\sqrt{\nu'(S)}, \quad \lambda_{3,4} = \pm\sqrt{\eta'(I)}, \tag{15}$$

are always real as well as the two relaxation times $\tau_S = D_S/\nu'$ and $\tau_I = D_I/\eta'$ are positive, as expected. Furthermore, it has to be noticed that, in the limit case $\tau_S \to 0$ and $\tau_I \to 0$, the hyperbolic model (14) reduces to the corresponding parabolic one analyzed in Ref. [13].

In order to reduce the number of the parameters involved in the model, we rescale the governing equation (14) by introducing the following change of variables:

$$\begin{aligned}
&\tilde{x} = \sqrt{\frac{A}{D_I}}\, x, \quad \tilde{t} = At, \quad \widetilde{S} = S, \quad \widetilde{I} = I,\\
&\widetilde{J^S} = \sqrt{\frac{1}{AD_I}}\, J^S, \quad \widetilde{J^I} = \sqrt{\frac{1}{AD_I}}\, J^I,\\
&\widetilde{\nu} = \frac{1}{AD_I}\nu, \quad \widetilde{\eta} = \frac{1}{AD_I}\eta, \quad \widetilde{\beta} = \frac{\beta}{A},\\
&\widetilde{\mu} = \frac{\mu}{A}, \quad \widetilde{D} = \frac{D_S}{D_I},
\end{aligned} \tag{16}$$

so that, by dropping the tilde notation for convenience, the system (14) can be recast as

$$\begin{aligned}
&\frac{\partial S}{\partial t} + \frac{\partial J^S}{\partial x} = 1 - S - \beta S I^2 = f(S,I),\\
&\frac{\partial I}{\partial t} + \frac{\partial J^I}{\partial x} = \beta S I^2 - (1+\mu) I = g(S,I),\\
&\frac{\partial J^S}{\partial t} + \nu' \frac{\partial S}{\partial x} = -\frac{\nu'}{D} J^S,\\
&\frac{\partial J^I}{\partial t} + \eta' \frac{\partial I}{\partial x} = -\eta' J^I,
\end{aligned} \tag{17}$$

where the rescaled relaxation times become $\tau_S = D/\nu'$ and $\tau_I = 1/\eta'$.

III. LINEAR STABILITY AND BIFURCATION ANALYSIS

The system of field equations (17) admits three different homogeneous steady states of the form $E^* = (S^*, I^*, 0, 0)$, which are

$$\begin{aligned}
&E_1^* = (1,0,0,0), \quad E_2^* = \left(\frac{\beta+\sqrt{\Delta}}{2\beta}, \frac{\beta-\sqrt{\Delta}}{2\beta(1+\mu)}, 0, 0\right),\\
&E_3^* = \left(\frac{\beta-\sqrt{\Delta}}{2\beta}, \frac{\beta+\sqrt{\Delta}}{2\beta(1+\mu)}, 0, 0\right),
\end{aligned} \tag{18}$$

with $\Delta = \beta^2 - 4\beta(1+\mu)^2$. The disease-free equilibrium state E_1^* always exists, whereas the two endemic states E_2^* and E_3^* are meaningful iff $\Delta \geqslant 0$, that is, for $\beta \geqslant \beta_{\rm ex} = 4(1+\mu)^2$. These equilibria are graphically represented in Fig. 1 in the S-I phase plane as intersections of the nullclines $f(S,I) = 0$ (continuous line) and $g(S,I) = 0$ (dashed line). In particular, two qualitatively different scenarios are shown: in Fig. 1(a), corresponding to $\beta = 20 < \beta_{\rm ex}$, the only equilibrium state is the disease-free configuration E_1^*, which results from the unique intersection between the nullclines; in Fig. 1(b), obtained for $\beta = 80 > \beta_{\rm ex}$, the nullclines exhibit three intersection points corresponding to the three steady states (18).

The subsequent analysis is devoted to give an insight into the behavior of these equilibria with respect to uniform and nonuniform perturbations by assuming μ and β as control parameters.

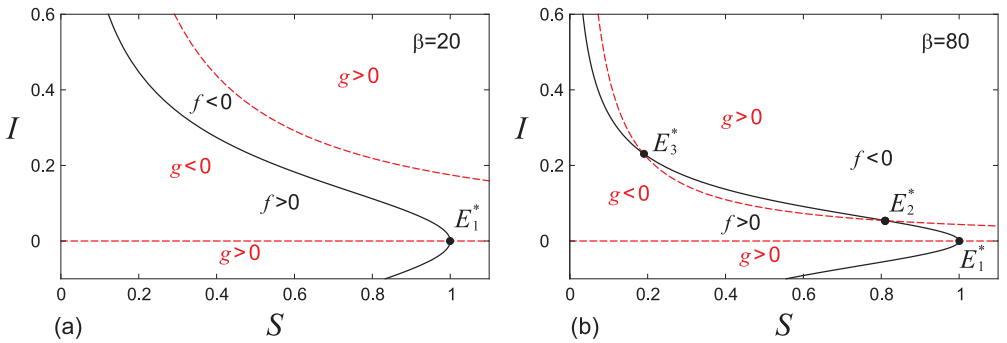

FIG. 1. (Color online) Nullclines $f(S,I) = 0$ (solid line) and $g(S,I) = 0$ (dashed line) obtained for $\mu = 2.5$.

A. Spatially homogeneous perturbations

The local stability of the homogeneous steady states E^* under small spatially independent perturbations can be determined by the sign of the eigenvalues σ of the following Jacobian matrix:

$$\begin{bmatrix} f_S^* & f_I^* & 0 & 0 \\ g_S^* & g_I^* & 0 & 0 \\ 0 & 0 & -\frac{\nu'^*}{D} & 0 \\ 0 & 0 & 0 & -\eta'^* \end{bmatrix}, \tag{19}$$

where the subscript stands for the partial derivative with respect to the indicated variable and the asterisk denotes that the functions are evaluated at E^*.

It is easy to check that two eigenvalues $\sigma_1 = -\nu'^*/D$ and $\sigma_2 = -\eta'^*$ are always negative according to (13), whereas the other two eigenvalues are solutions of the equation

$$\sigma^2 - (f_S^* + g_I^*)\sigma + (f_S^* g_I^* - f_I^* g_S^*) = 0, \tag{20}$$

so that the stability of the steady states is ensured iff the following conditions hold:

$$f_S^* + g_I^* < 0, \tag{21}$$

$$f_S^* g_I^* - f_I^* g_S^* > 0. \tag{22}$$

By evaluating these functions at the disease-free equilibrium E_1^*, we obtain

$$\begin{aligned} &f_S(E_1^*) = -1 < 0, \quad f_I(E_1^*) = 0, \quad g_S(E_1^*) = 0, \\ &g_I(E_1^*) = -(1+\mu) < 0, \end{aligned} \tag{23}$$

and it turns out that E_1^* is always stable. This result is consistent with our choice of the nonlinear incidence rate since, for small enough I, the nonlinear term $\beta S I^2$ does not yield a significant contribution.

For what concerns the endemic equilibria E_2^* and E_3^*, we have

$$\begin{aligned} &f_S^* = -\frac{\beta}{1+\mu} I^* < 0, \quad f_I^* = -2(1+\mu) < 0, \\ &g_S^* = \beta I^{*2} > 0, \quad g_I^* = 1 + \mu > 0. \end{aligned} \tag{24}$$

Therefore, E_2^* turns out to be unstable because the condition (22) is always violated, while the character of E_3^* depends upon the value of the control parameters. In particular, since (22) evaluated at E_3^* is always satisfied, its stability is determined by (21), namely,

$$E_3^* \text{ stable for } \begin{cases} \mu \leqslant 1, & \forall \beta, \\ \mu > 1, & \beta > \beta_{\rm cr}, \end{cases} \tag{25}$$

where

$$\beta_{\rm cr} = \frac{(1+\mu)^4}{\mu} > \beta_{\rm ex}. \tag{26}$$

Consequently, for $\mu > 1$, E_3^* changes its stability character as a function of β. It is interesting to notice that such a transition takes place through a Hopf bifurcation. Indeed, when $f_S^* + g_I^* = 0$, the characteristic equation (20) admits a pair of purely imaginary conjugate roots for $\beta = \beta_{\rm cr}$, and the transversality condition

$$\left.\frac{d\,\mathrm{Re}\,(\sigma)}{d\beta}\right|_{\beta_{\rm cr}} = -\frac{\mu^2}{2(1+\mu)^3(\mu-1)} \neq 0 \tag{27}$$

is fulfilled. Thus, system (17) undergoes a Hopf bifurcation at E_3^* to a spatially uniform periodic solution whose angular frequency $\delta = \sqrt{\mu^2 - 1}$ is determined by substituting $\sigma = i\delta$ into Eq. (20) at $\beta = \beta_{\rm cr}$.

It should be mentioned that the results hitherto obtained are in agreement with the ones proposed in Refs. [28,29].

B. Spatially nonhomogeneous perturbations

In the case of spatially dependent perturbations, the hyperbolic system (17) is linearized around E^* by looking for solutions of the form

$$\begin{aligned} S &= S^* + \bar{S}\exp(\sigma t + ikx), \\ I &= I^* + \bar{I}\exp(\sigma t + ikx), \\ J^S &= \bar{J}^S \exp(\sigma t + ikx), \\ J^I &= \bar{J}^I \exp(\sigma t + ikx), \end{aligned} \tag{28}$$

where k is the wave number. Then the resulting system

$$\begin{bmatrix} \sigma - f_S^* & -f_I^* & ik & 0 \\ -g_S^* & \sigma - g_I^* & 0 & ik \\ ik\nu'^* & 0 & \sigma + \frac{\nu'^*}{D} & 0 \\ 0 & ik\eta'^* & 0 & \sigma + \eta'^* \end{bmatrix} \begin{bmatrix} \bar{S} \\ \bar{I} \\ \bar{J}^S \\ \bar{J}^I \end{bmatrix} = \mathbf{0} \tag{29}$$

admits a nontrivial solution iff

$$\begin{aligned} &\left[\sigma^2 - \left(f_S^* - \frac{\nu'^*}{D}\right)\sigma + \left(k^2 - \frac{f_S^*}{D}\right)\nu'^*\right] \\ &\quad \times [\sigma^2 - (g_I^* - \eta'^*)\sigma + (k^2 - g_I^*)\eta'^*] \\ &\quad - \left(\sigma + \frac{\nu'^*}{D}\right)(\sigma + \eta'^*) f_I^* g_S^* = 0. \end{aligned} \tag{30}$$

As it is well known, if the real parts of all the roots of the characteristic equation (30) are negative for every wave number k, then the equilibrium state is linearly stable.

It is easy to ascertain that, taking into account (23), Eq. (30) can be straightforwardly factorized at E_1^* and all its roots exhibit negative real part $\forall k$, so that E_1^* preserves the same stability character found in the case of uniform perturbations.

On the other hand, the polynomial (30), evaluated at the endemic states E_2^* and E_3^*, can be rewritten in the general form

$$\sigma^4 + B_1\sigma^3 + B_2\sigma^2 + B_3\sigma + B_4 = 0, \tag{31}$$

where

$$\begin{aligned} B_1 &= \eta'^* + \frac{\nu'^*}{D} - f_S^* - g_I^*, \\ B_2 &= k^2(\nu'^* + \eta'^*) - \left(\eta'^* + \frac{\nu'^*}{D}\right)(f_S^* + g_I^*) \\ &\quad + \frac{\eta'^*\nu'^*}{D} + f_S^* g_I^* - f_I^* g_S^*, \end{aligned}$$

$$
\begin{aligned}
B_3 &= k^2\left[\nu'^*(\eta'^* - g_I^*) + \eta'^*\left(\frac{\nu'^*}{D} - f_S^*\right)\right] \\
&\quad - \frac{\nu'^*}{D} f_S^*(\eta'^* - g_I^*) - \eta'^* g_I^*\left(\frac{\nu'^*}{D} - f_S^*\right) \\
&\quad - \left(\eta'^* + \frac{\nu'^*}{D}\right) f_I^* g_S^*, \\
B_4 &= \nu'^*\eta'^*\left[k^4 - k^2\left(g_I^* + \frac{f_S^*}{D}\right) + \frac{f_S^* g_I^* - f_I^* g_S^*}{D}\right].
\end{aligned}
\tag{32}
$$

The stability of these equilibria can be thus discussed by using the Routh-Hurwitz criterion, which asserts that Eq. (31) admits all solutions with negative real parts iff the conditions

$$
B_1 > 0, \quad B_3 > 0, \quad B_4 > 0, \quad B_1 B_2 B_3 > B_3^2 + B_1^2 B_4 \tag{33}
$$

are verified $\forall k$.

The instability of the equilibrium E_2^* is easily determined since, as proved in the previous subsection, there exists at least a value of k ($k = 0$) at which conditions (33) are violated.

On the other hand, for what concerns the character of E_3^*, bearing in mind that $\nu'^*/D = 1/\tau_S \gg 1$ and $\eta'^* = 1/\tau_I \gg 1$, the evaluation of (33) is carried out by retaining the corresponding leading terms only. Such an analysis leads to

$$
\begin{cases}
B_1 > 0 & \text{for} \quad \forall \mu, \beta, \\
B_3 > 0 & \text{for} \quad \begin{cases} \mu \leqslant 1 & \forall \beta \\ \mu > 1 & \beta > \beta_{\mathrm{cr}}, \end{cases} \\
B_1 B_2 B_3 > B_3^2 + B_1^2 B_4 & \\
B_4 > 0 & \text{for} \quad \forall \mu, \quad \beta > \beta_{\mathrm{T}},
\end{cases}
\tag{34}
$$

where

$$
\beta_{\mathrm{T}} = \frac{D\widehat{\mu}^3[8 + 7D\widehat{\mu} + 3\widehat{\mu}^2 D^2 - 2(2 + D\widehat{\mu})\sqrt{2\widehat{\mu}D(\widehat{\mu}D - 1)}]}{(1 + D\widehat{\mu})^2}, \tag{35}
$$

with $\widehat{\mu} = \mu + 1$.

Since $\beta_{\mathrm{T}} > \beta_{\mathrm{cr}}$ as it follows from (26) and (35), E_3^* is asymptotically stable, for any value of μ, if $\beta > \beta_{\mathrm{T}}$.

By comparing the result reported in (25) with (34), we can conclude that in the region

$$
\begin{aligned}
&\mu \leqslant 1, \quad \beta_{\mathrm{ex}} < \beta < \beta_{\mathrm{T}}, \\
&\mu > 1, \quad \beta_{\mathrm{cr}} < \beta < \beta_{\mathrm{T}},
\end{aligned}
\tag{36}
$$

E_3^* is stable with respect to small homogeneous perturbations but becomes unstable to the inhomogeneous ones; namely, the system exhibits a diffusion-driven instability which is typically referred to as Turing instability.

As known, the onset of Turing bifurcation corresponds to the presence of a null root of the characteristic equation (31) for a value of $k \neq 0$, which is tantamount to requiring $B_4(k^2) = 0$. Therefore, from (34) it can be verified that this bifurcation takes place at $\beta = \beta_{\mathrm{T}}$ and that, in correspondence to such a value of the control parameter, the minimum of the biquadratic function $B_4(k^2) = 0$ defines the critical wave number k_{T} given by

$$
\begin{aligned}
k_{\mathrm{T}}^2 &= \frac{\beta_{\mathrm{T}} + \sqrt{\beta_{\mathrm{T}}^2 - 4\beta_{\mathrm{T}}^2\widehat{\mu}}}{4\beta_{\mathrm{T}}^2\widehat{\mu}} \\
&\quad \times \sqrt{\frac{2\beta_{\mathrm{T}}\widehat{\mu}}{D}\left(4\widehat{\mu}^2 - \beta_{\mathrm{T}} + \sqrt{\beta_{\mathrm{T}}^2 - 4\beta_{\mathrm{T}}\widehat{\mu}^2}\right)}.
\end{aligned}
\tag{37}
$$

This wave number is associated to the stationary spatial pattern generated as a consequence of the diffusion-driven instability when the control parameters cross the Turing bifurcation locus (35).

The complete bifurcation diagram in the μ-β plane, showing the behavior of the system with respect to uniform and nonuniform perturbations, is depicted in the top of Fig. 2 for $D = 6$. This choice corresponds to the setup shown in Ref. [13]. In particular, the bifurcation lines $\beta_{\mathrm{cr}}(\mu)$ and $\beta_{\mathrm{T}}(\mu)$, together with the curve $\beta_{\mathrm{ex}}(\mu)$, separate the parametric plane into four distinct domains. The dynamics occurring in region I are not taken into account since the endemic states are meaningless in there. On the other hand, the endemic state E_3^* is unconditionally unstable if it falls into domain II, defined by $\mu > 1$ and $\beta_{\mathrm{ex}} < \beta < \beta_{\mathrm{cr}}$. In this region, both Hopf and Turing instabilities can occur. In domain III, represented by (36), the steady state is stable with respect to homogeneous perturbations but loses its stability with respect to perturbations of given wave numbers k, so stationary inhomogeneous patterns can be here observed. Finally, in domain IV, corresponding to $\beta > \beta_{\mathrm{T}}$, E_3^* is stable with respect to both uniform and nonuniform perturbations.

In passing we note that the diagram shown in Fig. 2 slightly differs from the corresponding one reported in Fig. 1 of Ref. [13] since the Hopf bifurcation curve exhibits a different behavior in the region $\mu < 1$, so that the domain labeled "I" in Ref. [13], where the system should be destabilized by homogeneous oscillations only, does not occur in our model.

These results can be confirmed by investigating numerically the characteristic equation (31). In particular, since (31) always admits two negative real roots, hereafter it is possible to focus the attention on the properties of the other two roots only. Therefore, by setting the rescaled recovery rate at $\mu = 2.5$ and considering $\nu'^* = \eta'^* = 10^5$, in the bottom of Fig. 2 we depict the character of these roots in correspondence of the points labeled A–F (shown in the top of Fig. 2), which are representative of qualitatively different dynamical behaviors of the endemic state E_3^*. In detail, at point F, all the roots present negative real part independently of k, namely, the system is unconditionally stable. We checked that such a behavior also holds in the region labeled "I" of Ref. [13], in agreement with our theoretical predictions. On the other hand, at point E, the characteristic equation (31) exhibits a null root for $k = k_{\mathrm{T}} \neq 0$

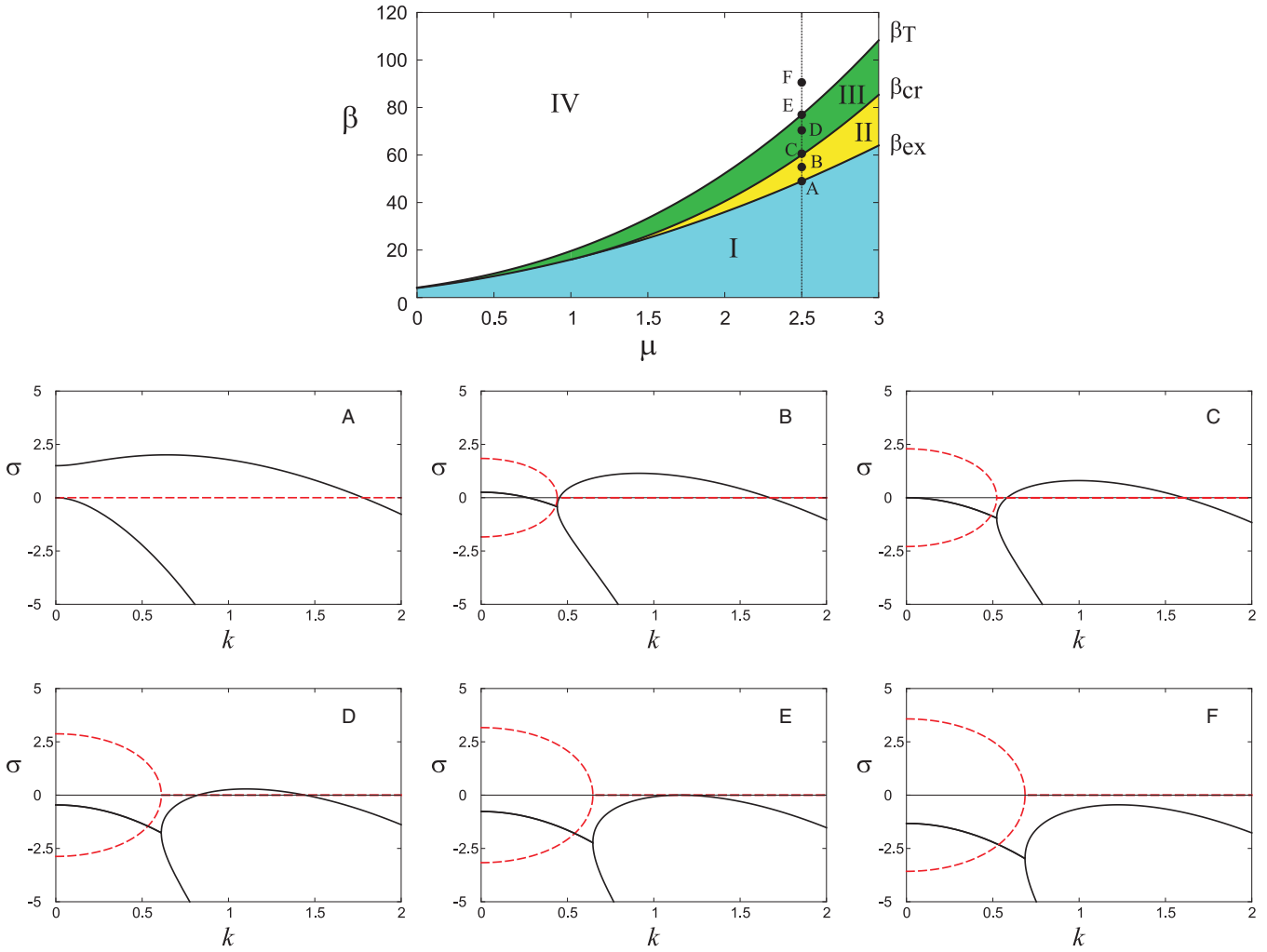

FIG. 2. (Color online) (Top) Bifurcation diagram related to the endemic state E_3^* in the μ-β parametric plane. The bottom figures are representative of the real (solid line) and the imaginary (dotted lines) parts of two roots of (31) evaluated at the points (A–F), which lie along the vertical dotted line indicated in the top figure.

and all the other roots with negative real part. This situation corresponds to the onset of Turing bifurcation. Crossing the bifurcation line $\beta_T(\mu)$, namely, at point D, we observe a finite range of wave numbers (not including $k = 0$) in which (31) admits a positive real root. This interval corresponds to the Turing instability region. By moving from point D to B, a pair of complex conjugate roots reverses the sign of its real part at $k = 0$ and thus manifests the occurrence of a Hopf bifurcation (point C). So, at point B, both Turing and Hopf instability arise. Finally, at point A, the system is fully destabilized by virtue of the existence of a large interval of k (including $k = 0$) where one root is always real and positive.

IV. NUMERICAL INTEGRATION OF THE GOVERNING EQUATIONS

The analytical results obtained in the previous section are now validated through the numerical integration of the governing system of differential equations (17). We present some numerical results which are representative of the different scenarios occurring as the control parameter β is varied. In particular, we fix $\mu = 2.5$ in order to explore the dynamics corresponding to the points labeled in Fig. 2. We also set the phenomenological parameters involved into the hyperbolic model $\nu'^* = \eta'^* = 10^5$ and, when spatial effects are taken into account, $D = 6$.

First, we investigate the dynamics occurring in region II by choosing $\beta = 55$ (corresponding to point B of Fig. 2) in the presence and in the absence of spatial effects, as shown in Fig. 3. In particular, the numerical solution of the nonspatial model (where all field variables do not depend on x) with initial conditions $S(0) = I(0) = 0.5$ is depicted in Fig. 3(a). It shows that, starting from an initial coexistence state, the system evolves in time approaching the disease-free configuration E_1^*, which, according to the analysis carried out in Sec. III A, is the only stable equilibrium state in this region. In Figs. 3(b) and 3(c), we integrate the spatially extended model (17) with periodic boundary conditions at $x = \pm 20$ and the following initial conditions:

$$S(0,x) = 0.5, \quad I(0,x) = \begin{cases} \alpha(1-x^2) & -1 < x < 1, \\ 0 & \text{otherwise}, \end{cases} \tag{38}$$

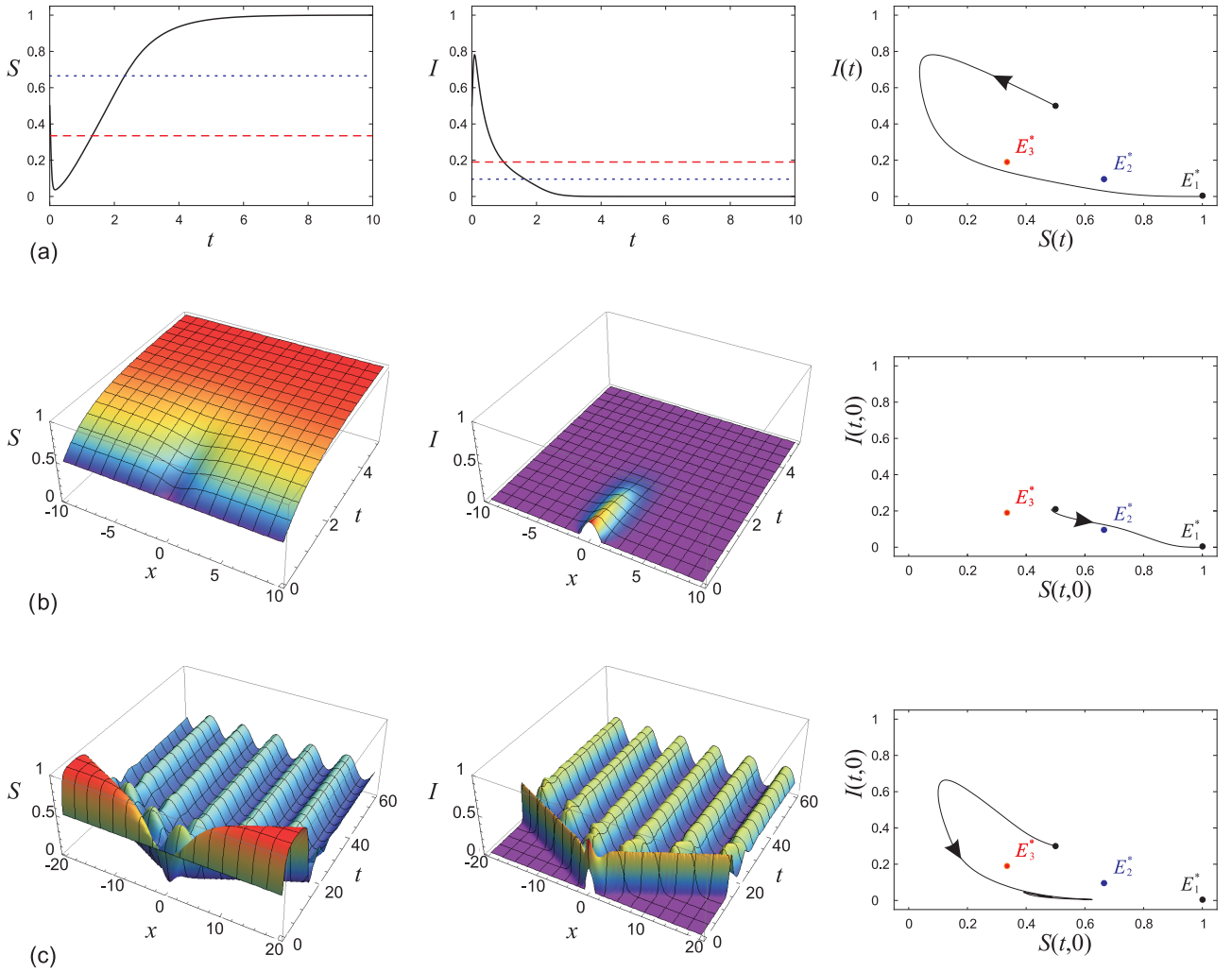

FIG. 3. (Color online) Dynamics observed at point B of Fig. 2. (a) Time evolution of susceptibles and infectives in the absence of diffusive effects. The dotted and the dashed lines are representative of the endemic states E_2^* and E_3^*, respectively. (b, c) Spatiotemporal evolution of susceptibles and infectives obtained in the presence of diffusive effects for $\alpha = 0.2$ (b) and $\alpha = 0.3$ (c). The corresponding trajectories described in the phase plane are also shown in the figures on the right.

where the parameter α defines the initial density of infectives at $x = 0$. Numerical results reveal a high sensitivity of the system to small variations of this latter parameter. For instance, in the case $\alpha = 0.2$, the system rapidly converges towards the disease-free equilibrium state [see Fig. 3(b)], whereas for a slightly larger initial density of infectives, namely, $\alpha = 0.3$, spatial patterns are observed as a consequence of Turing instability [see Fig. 3(c)].

Next, we investigate the dynamics occurring at the boundary between regions II and III (point C of Fig. 2, obtained for $\beta = \beta_{cr} = 60.025$), which corresponds to the onset of Hopf bifurcation in the nonspatial model. As can be noticed in Fig. 4, the trajectories described in the phase plane show the existence of an unstable limit cycle. In fact, by choosing as initial conditions a configuration which lies outside the limit cycle [Fig. 4(a)], the system spirals outwards until it reaches the stable disease-free state E_1^*. A periodic closed trajectory is observed only if the initial condition is chosen along the limit cycle [Fig. 4(b)]. Also, it should be mentioned that the period of the time oscillations computed numerically, $\Delta t = 2.75$, is in very good agreement with the analytical one found in Sec. III A, $\Delta t = 2\pi/\sqrt{\mu^2 - 1} = 2.74$.

In domain III, constrained between Hopf and Turing bifurcation lines, both equilibria E_1^* and E_3^* are found to be stable with respect to homogenous perturbations so that all trajectories converge to one of these steady states depending on the initial conditions. More precisely, by choosing $\beta = 70$ (corresponding to point D) and two sets of initial conditions having the same value of susceptibles, $S(0) = 0.5$, but slightly different values of infectives, $I(0) = 0.09$ and $I(0) = 0.1$, the system tends to E_1^* and E_3^*, respectively [see Figs. 5(a) and 5(b)]. In the same region, we also integrated the spatial model (17) with the same kind of boundary and initial conditions used in Figs. 3(b) and 3(c). Numerical integration of the governing equations shows that, by choosing $\alpha = 0.15$, the system approaches in time the uniform steady state E_1^*, which, thus, preserves the stability character deduced in the presence of nonuniform perturbations [see Fig. 5(c)]. On the other hand, increasing slightly the value of α, namely, $\alpha = 0.2$, spatial patterns around E_3^* are observed [see Fig. 5(d)].

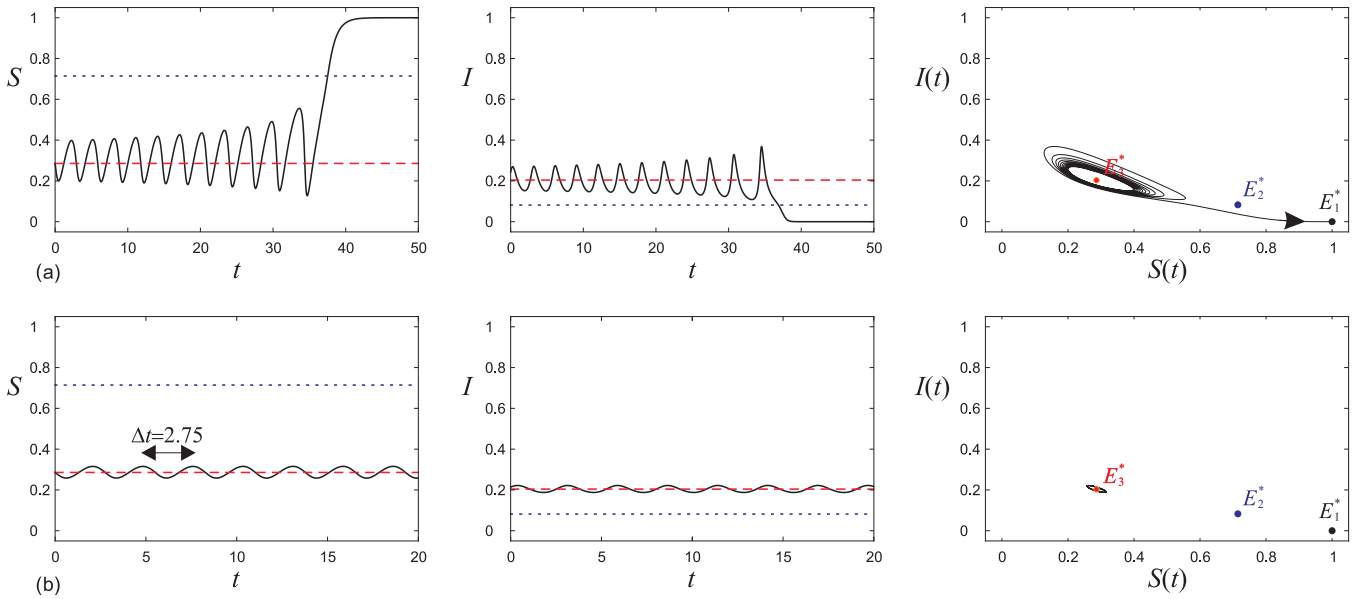

FIG. 4. (Color online) Dynamics observed at point C of Fig. 2. The figures in the first two columns show the time evolution of susceptibles and infectives, respectively, whereas the figures in the last column represent the corresponding trajectories on the phase plane. The initial conditions are (a) $S(0) = 0.307 \equiv S|_{E_3^*}$, $I(0) = 0.244 > I|_{E_3^*}$; (b) $S(0) = 0.307 \equiv S|_{E_3^*}$, $I(0) = 0.214 > I|_{E_3^*}$.

We would like to mention that such patterns are analogously generated by choosing several other typologies of initial and boundary conditions. The results hitherto obtained also reveal that, contrary to what one could expect, in the model under investigation, the occurrence of Turing patterns depends upon the choice of initial conditions. This behavior is justified by the existence of an unconditionally stable steady state, E_1^*, within the same Turing region.

For $\beta = \beta_T = 76.959$, namely, at the Turing threshold (point E), the system gives rise to a waveform stationary in time and oscillatory in space similar to the one depicted in Fig. 5(d). The wavelength $\lambda_T = 5.67$ associated to this pattern agrees quite well with the analytical one $2\pi/k_T = 5.46$ obtained by using (37) (see Fig. 6).

Finally, crossing upward the Turing bifurcation curve, and so entering region IV, the qualitative behavior of the equilibrium E_3^* changes and the spatial symmetry of the system is restored. In fact, both steady states E_1^* and E_3^* are here unconditionally stable, and thus, according to the choice of initial conditions, the system converges towards one of these equilibria, as shown in Fig. 7 (obtained for $\beta = 80$, corresponding to point F).

V. TRAVELING WAVE SOLUTIONS

In this section we get an insight into the behavior of traveling wave solutions admitted by the system (17).

From the biological viewpoint, such solutions represent spatial patterns of the distribution of the infection in the population which propagate at a certain speed as a wave through, for instance, the conversion of part of the susceptibles into infected ones. In other words, traveling wave solutions describe the mechanism by which a wave of infection advances and invades the susceptible population.

Therefore, we look for solutions of the form $S = S(z)$, $I = I(z)$, $J^S = J^S(z)$, $J^I = J^I(z)$, where $z = x - Vt$ is the wave coordinate and $V > 0$ is the constant wave speed. This requirement leads to the following set of ordinary differential equations:

$$\begin{aligned} -V\frac{dS}{dz} + \frac{dJ^S}{dz} &= f(S,I), \\ -V\frac{dI}{dz} + \frac{dJ^I}{dz} &= g(S,I), \\ -V\frac{dJ^S}{dz} + \nu'\frac{dS}{dz} &= -\frac{\nu'}{D}J^S, \\ -V\frac{dJ^I}{dz} + \eta'\frac{dI}{dz} &= -\eta' J^I, \end{aligned} \tag{39}$$

which obviously admits the same steady states (18) of the hyperbolic model (17).

Since any traveling wave front solution must be a heteroclinic orbit in the phase space that links two steady states, we first consider the linear stability of these equilibria with respect to z by assuming

$$\begin{aligned} S &= S^* + \hat{S}e^{\chi z}, \quad I = I^* + \hat{I}e^{\chi z}, \\ J^S &= \hat{J}^S e^{\chi z}, \quad J^I = \hat{J}^I e^{\chi z}, \end{aligned} \tag{40}$$

so that the (39) is recast as

$$\begin{bmatrix} -V\chi - f_S^* & -f_I^* & \chi & 0 \\ -g_S^* & -V\chi - g_I^* & 0 & \chi \\ \chi\nu'^* & 0 & -V\chi + \frac{\nu'^*}{D} & 0 \\ 0 & \chi\eta'^* & 0 & -V\chi + \eta'^* \end{bmatrix} \times \begin{bmatrix} \hat{S} \\ \hat{I} \\ \hat{J}^S \\ \hat{J}^I \end{bmatrix} = \mathbf{0}. \tag{41}$$

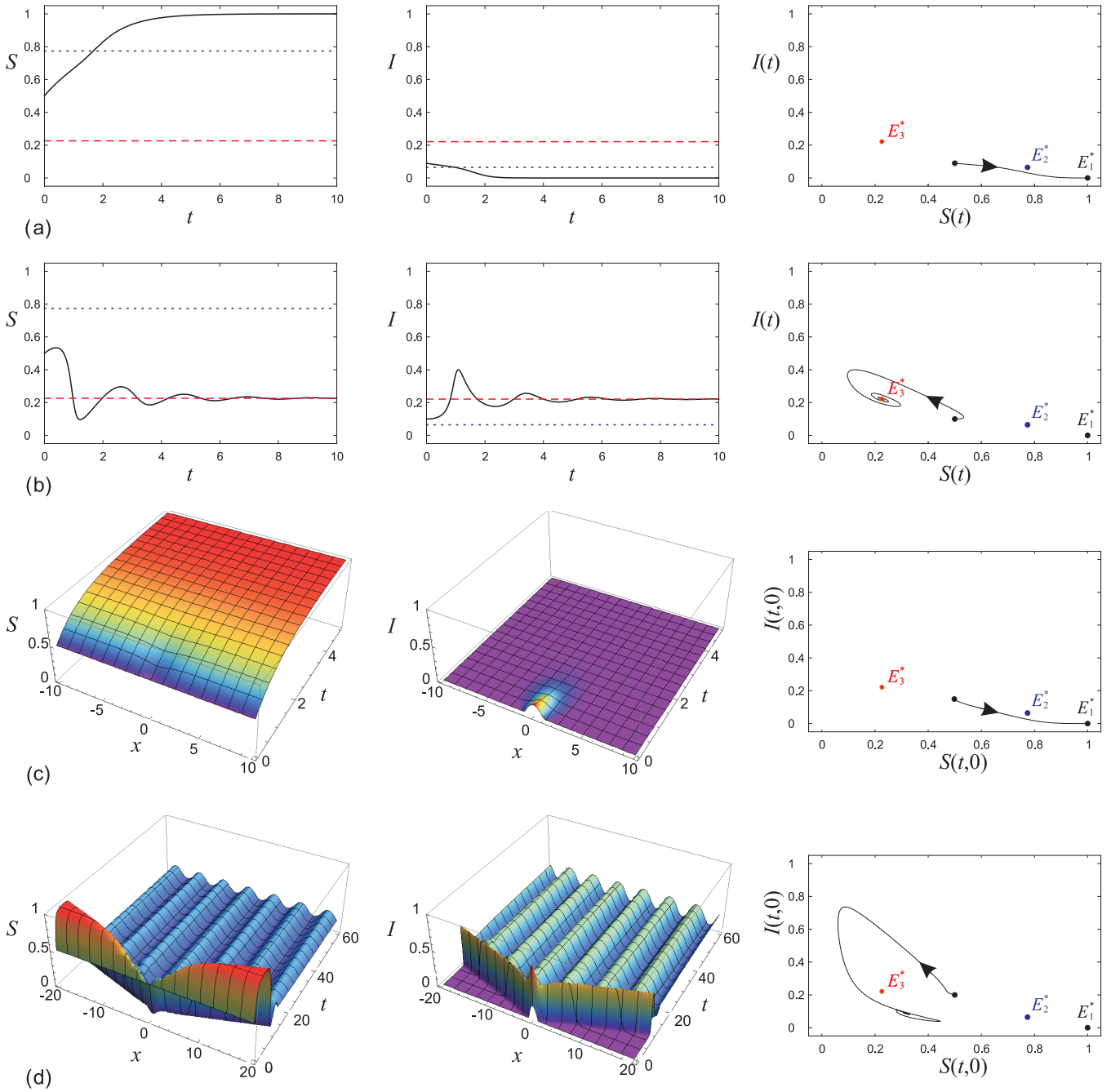

FIG. 5. (Color online) Dynamics observed at point D of Fig. 2. (a, b) Time evolution of susceptibles and infectives in the absence of diffusive effects obtained by using different initial conditions for the infectives, namely, $I(0) = 0.09$ (a) and $I(0) = 0.1$ (b). The dotted and the dashed lines are representative of the endemic states E_2^* and E_3^*, respectively. (c, d) Spatiotemporal evolution of susceptibles and infectives obtained in the presence of diffusive effects for $\alpha = 0.15$ (c) and $\alpha = 0.2$ (d). The corresponding trajectories described in the phase plane are also shown in the figures on the right.

Nontrivial solutions of the linearized system (41) are found iff χ satisfies the following characteristic equation:

$$\left[(\nu'^* - V^2)\chi^2 - \left(f_S^* - \frac{\nu'^*}{D}\right)V\chi + f_S^*\frac{\nu'^*}{D}\right] \times [(\eta'^* - V^2)\chi^2 - (g_I^* - \eta'^*)V\chi + g_I^*\eta'^*] - \left(V\chi - \frac{\nu'^*}{D}\right)(V\chi - \eta'^*)f_I^* g_S^* = 0. \quad (42)$$

Evaluating (42) at E_1^* and taking into account (23), it is easy to ascertain that the disease-free equilibrium is always unstable. In fact, the roots of (42), given by

$$\chi_{1,2}(E_1^*) = \frac{-\left(1 + \frac{\nu'^*}{D}\right)V \pm \sqrt{\left(1 - \frac{\nu'^*}{D}\right)^2 V^2 + 4\frac{\nu'^{*2}}{D}}}{2(\nu'^* - V^2)},$$
$$\chi_{3,4}(E_1^*) = \frac{-(\widehat{\mu} + \eta'^*)V \pm \sqrt{(\widehat{\mu} - \eta'^*)^2 V^2 + 4\widehat{\mu}\eta'^{*2}}}{2(\eta'^* - V^2)}, \quad (43)$$

are real and, in particular, at least two of them are positive.

For what concerns the coexistence equilibria E_2^* and E_3^*, the characteristic equation (42) can be rewritten in the general form

$$(V\chi)^4 + C_1(V\chi)^3 + C_2(V\chi)^2 + C_3 V\chi + C_4 = 0, \tag{44}$$

being

$$C_1 = \frac{1}{\left(1-\frac{\nu'^*}{V^2}\right)\left(1-\frac{\eta'^*}{V^2}\right)}\left[\left(1-\frac{\nu'^*}{V^2}\right)(g_I^*-\eta'^*)+\left(1-\frac{\eta'^*}{V^2}\right)\left(f_S^*-\frac{\nu'^*}{D}\right)\right], \tag{45}$$

$$C_2 = \frac{1}{\left(1-\frac{\nu'^*}{V^2}\right)\left(1-\frac{\eta'^*}{V^2}\right)}\left[\left(f_S^*-\frac{\nu'^*}{D}\right)(g_I^*-\eta'^*)-\left(1-\frac{\nu'^*}{V^2}\right)g_I^*\eta'^*-\left(1-\frac{\eta'^*}{V^2}\right)f_S^*\frac{\nu'^*}{D}-f_I^*g_S^*\right], \tag{46}$$

$$C_3 = \frac{1}{\left(1-\frac{\nu'^*}{V^2}\right)\left(1-\frac{\eta'^*}{V^2}\right)}\left[f_I^*g_S^*\left(\frac{\nu'^*}{D}+\eta'^*\right)-\left(f_S^*-\frac{\nu'^*}{D}\right)g_I^*\eta'^*-(g_I^*-\eta'^*)f_S^*\frac{\nu'^*}{D}\right], \tag{47}$$

$$C_4 = \frac{1}{\left(1-\frac{\nu'^*}{V^2}\right)\left(1-\frac{\eta'^*}{V^2}\right)}\frac{(f_S^*g_I^*-f_I^*g_S^*)\eta'^*\nu'^*}{D}. \tag{48}$$

Therefore, the stability of these equilibria will be again investigated by using the Routh-Hourwitz criterion and taking into account the hyperbolic nature of the model under consideration through the assumptions $V^2 \ll \min\{\nu'^*,\eta'^*\}$ and $g_I^* \ll \eta'^*$.

From a direct inspection of (48), it results that E_2^* is always asymptotically unstable, being $C_4 < 0$ for any choice of the control parameters.

For the coexistence state E_3^*, we see that, while $C_1 > 0$ and $C_4 > 0$ are always verified, the other two conditions, $C_3 > 0$ and $C_1C_2C_3 > C_3^2 + C_1^2C_4$, lead to restrictions on both the control parameters and the wave speed. In detail, the asymptotical stability of E_3^* is ensured only in the region $\mu > 1$ iff

$$\begin{aligned} &\beta_{ex} < \beta < \beta_{TW} \quad \text{for} \quad V^2 \ll \min\{\nu'^*,\eta'^*\},\\ &\beta_{TW} < \beta < \beta_{cr} \quad \text{for} \quad V_{TW}^2(\beta,\mu) < V^2 \ll \min\{\nu'^*,\eta'^*\}, \end{aligned} \tag{49}$$

being

$$\begin{aligned} \beta_{TW} = \frac{\hat\mu^3}{(1+D\hat\mu)^2}\{&(D+1)^2[(\hat\mu D+1)^2+1]-\hat\mu D^2(\hat\mu D+1)\\ &-D(D+1)(\hat\mu D+2)\sqrt{\hat\mu[\hat\mu(D^2+1)-2]}\}, \end{aligned} \tag{50}$$

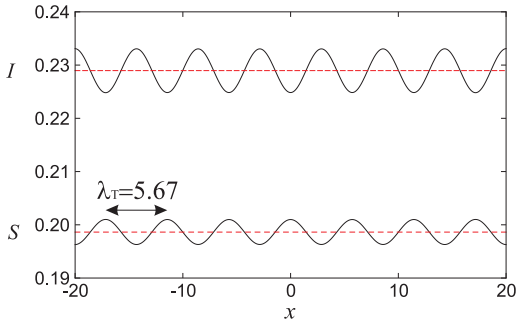

FIG. 6. (Color online) Dynamics observed at point E of Fig. 2, namely, at the Turing threshold. The figure depicts the stationary pattern originated around E_3^* together with its characteristic wavelength.

$$V_{TW}^2(\beta,\mu) = -\frac{(f_S^*-g_I^*D)^2+f_I^*g_S^*(D+1)^2}{(D+1)(f_S^*+g_I^*)}, \tag{51}$$

where the critical value of the wave speed in (51) is obtained from the condition $C_1C_2C_3 - C_3^2 - C_1^2C_4 = 0$. Therefore, it is possible to conclude that if the control parameter β lies in the range $\beta_{ex} < \beta < \beta_{TW}$ [region T_1 in Fig. 8(a)], the stability of a traveling wave connecting the endemic state E_3^* with one of the other unstable states is guaranteed if the wave speed does not exceed the upper bound given by $\min\{\sqrt{\nu'^*},\sqrt{\eta'^*}\}$. On the other hand, a traveling wave solution can be also observed in the range $\beta_{TW} < \beta < \beta_{cr}$ [region T_2 in Fig. 8(a)], provided that the wave speed overcomes the threshold $V_{TW}(\beta,\mu)$ but does not overtake the previous upper bound. These results suggest the possibility to build up a stability diagram in the V-β plane, as in Fig. 8(b), where the curve here depicted represents the function $V_{TW}(\beta,\mu)$ evaluated at $\mu = 2.5$.

As can be verified, the characteristic equation (44) admits a pair of purely imaginary roots $V\chi = i\omega$ under the following constraints:

$$\omega^2 = \frac{C_3}{C_1}, \tag{52}$$

$$C_1C_2C_3 = C_3^2 + C_1^2C_4, \tag{53}$$

so that (53) defines the Hopf bifurcation locus in the V-β plane, which coincides with the curve represented in Fig. 8(b). In fact, since the transversality condition is numerically verified to be fulfilled, when the bifurcation locus (53) is crossed, the system (39) undergoes a Hopf bifurcation at E_3^* to a small amplitude periodic solution, which corresponds to a traveling wave solution of the hyperbolic system (17).

To validate these results, we carry out additional investigations by integrating numerically the system (39). In detail, we consider two sets of parameters, $(\beta,V) = (55,3)$ and $(52,3)$, which identify, in the β-V parametric plane of Fig. 8(b), two qualitatively different classes of dynamics occurring below and above the bifurcation locus (53), respectively.

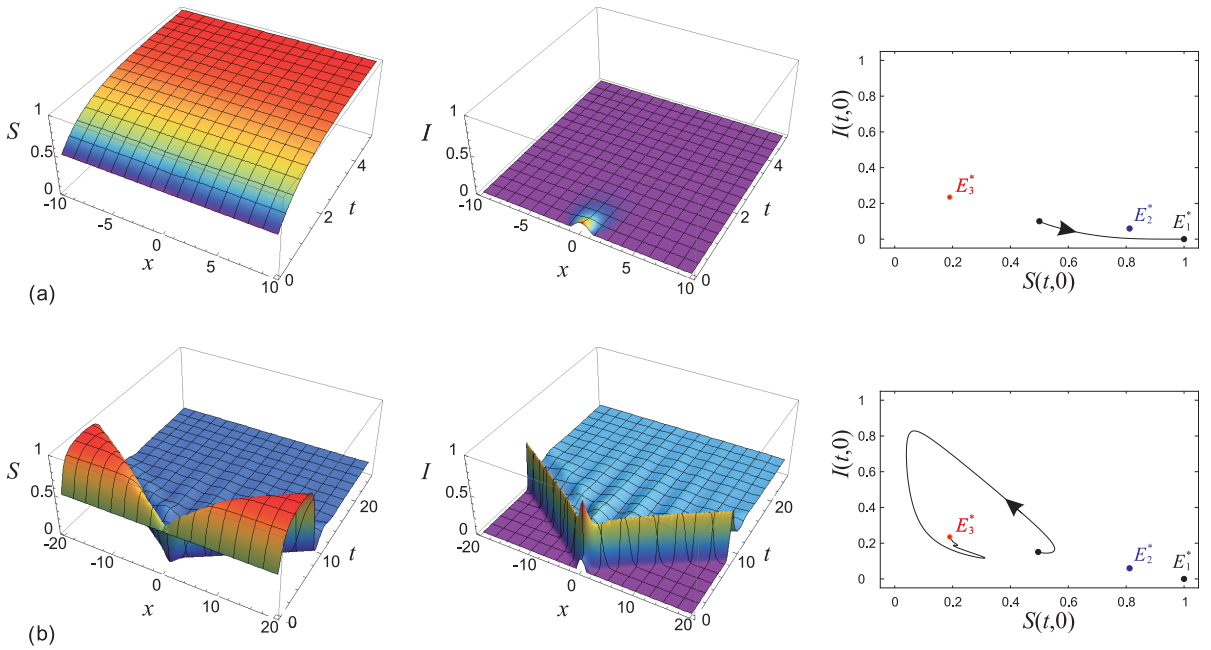

FIG. 7. (Color online) Dynamics observed at point F of Fig. 2 for $\alpha = 0.10$ (a) and $\alpha = 0.15$ (b).

Figure 9, obtained for $\beta = 55$, shows the impossibility to link two steady states with each other due to their instability character. Indeed, by choosing as initial condition the state E_1^* or E_2^*, the trajectory evolves in time toward the limit cycle without entering it [see Figs. 9(a) and 9(b)], whereas, starting from E_3^*, the system spirals outwards approaching the limit cycle from the interior [see Fig. 9(c)]. From a direct inspection of Fig. 9 one can thus conclude that the limit cycle is stable. On the other hand, the numerical results obtained for $\beta = 52$ reveal the possibility of generating a stable connection between two steady states, as depicted in Fig. 10. In particular, depending on the choice of the initial conditions, by fixing a point in space, two different scenarios can be observed as the front passes by. If a perturbation acts in the neighborhood of the disease-free state E_1^*, an observer would see the infected population growing from such an unstable zero to the stable endemic value $(I|_{E_3^*})$, as depicted in Fig. 10(a). Such a situation requires the initial dissipative fluxes to be large enough to overcome the smallness of the nonlinear incidence term $\beta S I^2$. On the other hand, if the configuration E_2^* is perturbed (even for zero initial dissipative fluxes), a spread of infectious disease can propagate as a wave from an endemic state to the other one; see Fig. 10(b). In particular, the connection between these latter equilibria exhibits an overshoot, which determines a surplus of infectives with respect to their final steady-state value, followed by a damped ringing, due to the presence of complex eigenvalues in (44).

VI. CONCLUSIONS

In this paper, along the leading ideas of extended thermodynamics, we derived a hyperbolic system of PDEs in order to describe the spread of disease in a population divided into three subgroups: the susceptible, the infected, and the removed individuals. In particular, it is assumed that the disease is transmitted according to a nonlinear convex incidence rate. The system of equations so obtained reduces to the parabolic

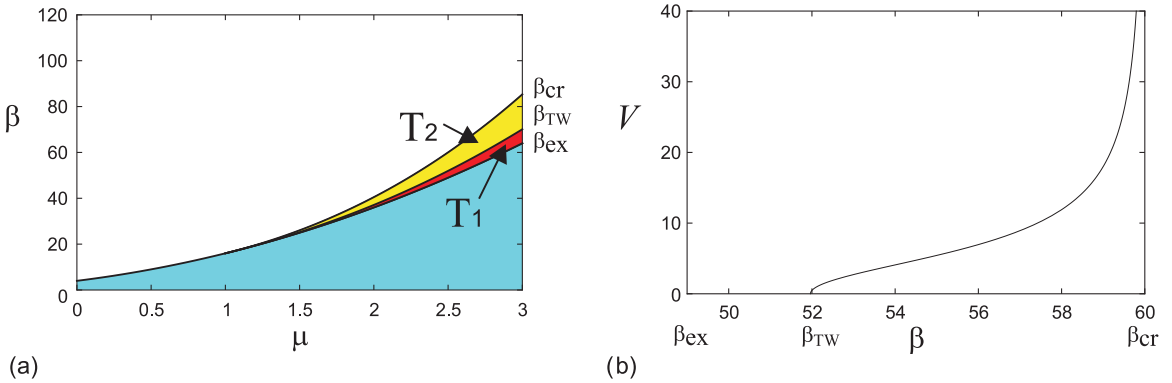

FIG. 8. (Color online) (a) Stability diagram in the μ-β parametric plane related to a traveling wave solution linking the endemic state E_3^* with one of the other steady states. (b) Bifurcation diagram in the β-V plane evaluated at $\mu = 2.5$.

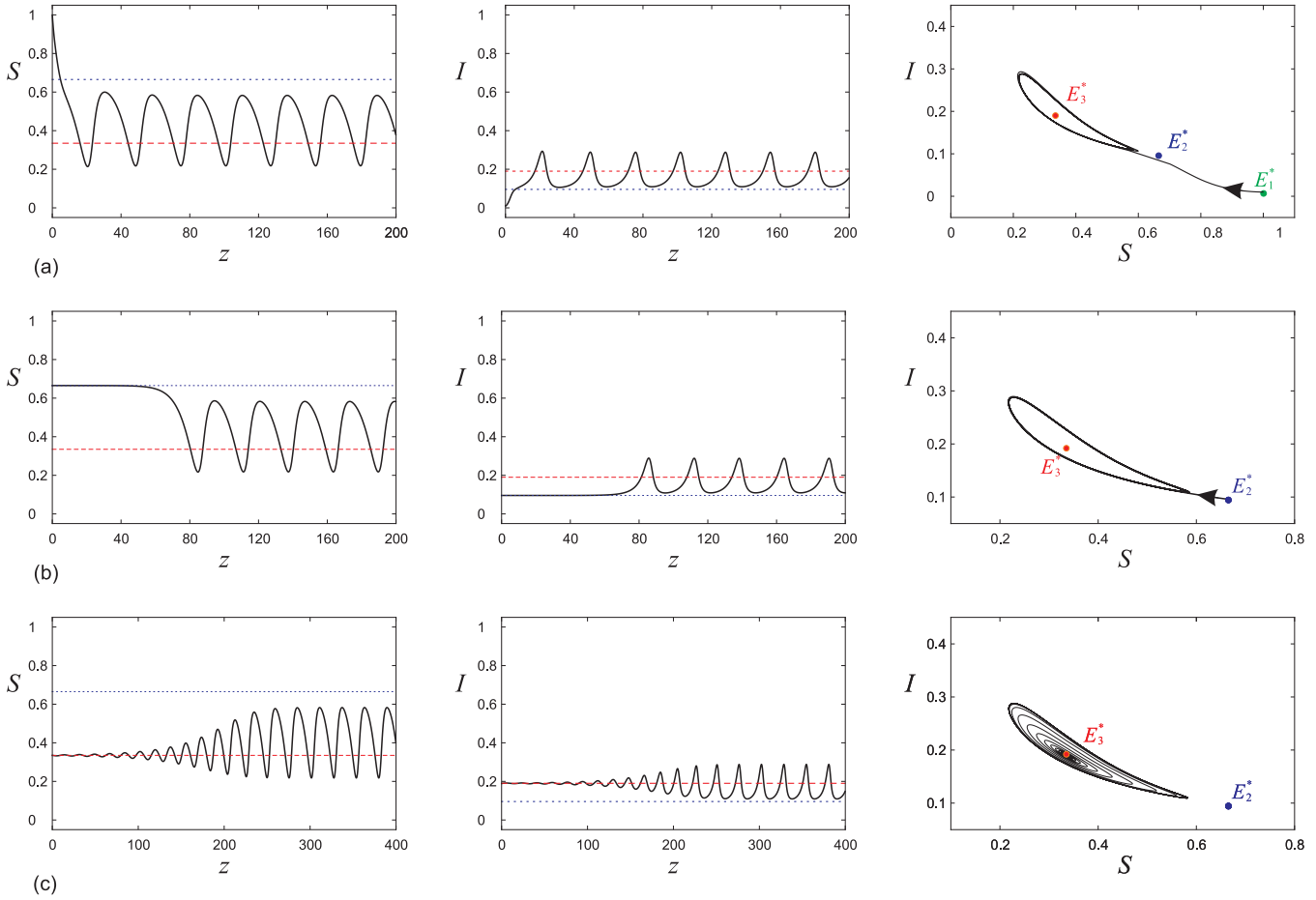

FIG. 9. (Color online) Numerical solution of system (39) for $(\beta, V) = (55,3)$ depicting the trajectories of the two species as a function of the wave coordinate z and in the S-I phase plane. The plots represent the evolution of the system from the unstable steady states E_1^* (a), E_2^* (b), or E_3^* (c) toward the stable limit cycle.

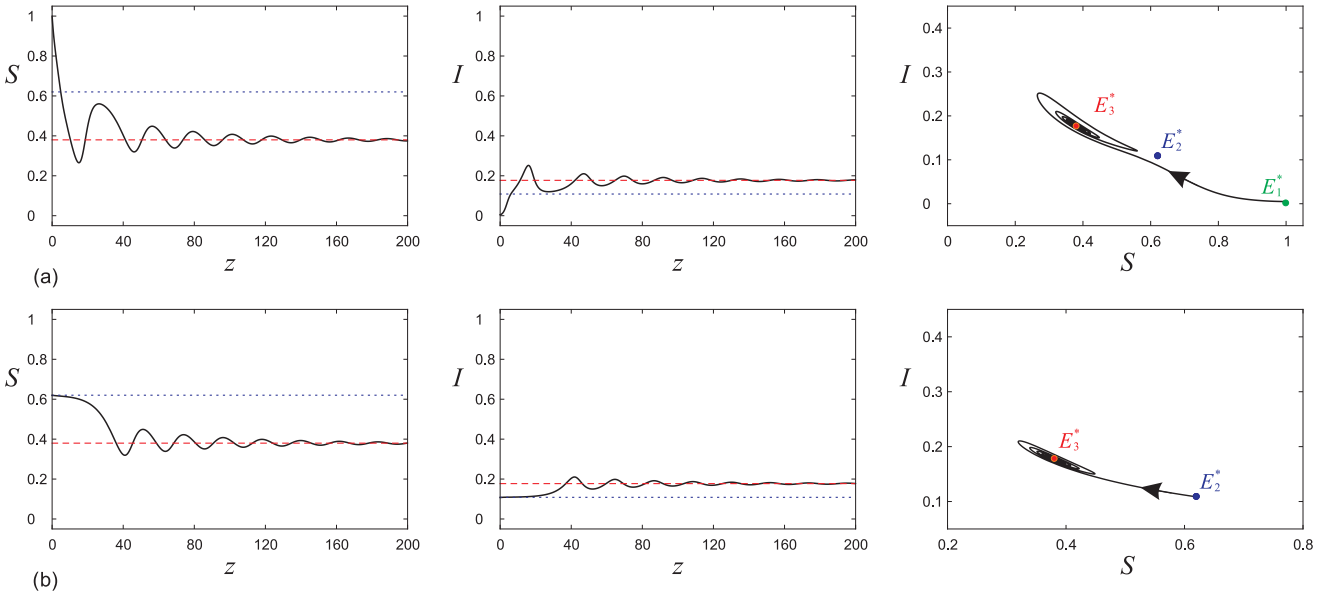

FIG. 10. (Color online) Numerical solution of system (39) for $(\beta, V) = (52,3)$ showing the stable connection (traveling wave) between E_1^* (a) or E_2^* (b) and E_3^*.

model considered in Ref. [13] when the relaxation times tend to zero.

Moreover, we carried out the linear stability analysis of the steady state solutions with respect to both homogeneous and nonhomogeneous perturbations in terms of two control parameters: the transmission rate and the recovery rate, both normalized with respect to the birth rate of the population. Analytical and numerical investigations showed that three equilibria are admitted by the model in point: the disease-free state, which is unconditionally stable, and two endemic states, one of which is always unstable while the other one changes its character according to the control parameter values. Consequently it has been possible to draw the corresponding stability diagram, which revealed some interesting features. The most evident one is related to the existence of two kinds of bifurcations, Hopf and Turing, which manifest themselves with the appearance of stable oscillations in time and in space, respectively. In particular, we demonstrated the existence of Turing patterns in a well-defined region of the parametric plane (36), slightly different with respect to the one found in Ref. [13]. In fact, it has been shown that the diffusion-driven instability occurs for any value of the recovery rate if the strength of the transmission rate is smaller than a critical value $\beta < \beta_{\mathrm{T}}$.

Also, since the infection can propagate as a wave, a study of the behavior of a traveling wave solution has been worked out. Our results revealed the existence of a critical transmission rate $\beta = \beta_{\mathrm{cr}}$ above which an epidemic wave cannot occur. In particular, for $\beta_{\mathrm{ex}} < \beta < \beta_{\mathrm{TW}}$, the infection spreads with a velocity subjected to an upper limit due to the hyperbolic nature of the model. On the other hand, for $\beta_{\mathrm{TW}} < \beta < \beta_{\mathrm{cr}}$, an epidemic wave moves through the population with a velocity lying between a lower and an upper bound. Biologically speaking, the perturbation of a linear habitat, which initially contains a smaller amount of infectives with respect to susceptibles, may thus propagate as an infectious wave moving across the population with a finite velocity and can even exhibit overshoot phenomena. Finally, our theoretical results are confirmed by numerical integration of the governing equations.

ACKNOWLEDGMENTS

The authors thank the anonymous referees for helpful comments and suggestions. This work was supported by INDAM-GNFM under the project entitled "Analisi qualitativa e stabilità in fluidodinamica e in modelli biologici discreti e continui."

[1] J. D. Murray, *Mathematical Biology I: An Introduction*, 3rd ed. (Springer, Berlin, 2003), pp. 315–394.
[2] J. D. Murray, *Mathematical Biology II: Spatial Models and Biomedical Applications*, 3rd ed. (Springer, Berlin, 2003), pp. 661–721.
[3] R. M. Anderson and R. M. May, *Infectious Diseases in Humans: Dynamics and Control* (Oxford University Press, Oxford, 1991).
[4] H. W. Hethcote, SIAM Rev. **42**, 599 (2000).
[5] F. M. Hilker and K. Schmitz, J. Theor. Biol. **255**, 299 (2008).
[6] L. J. S. Allen, Lect. Notes Math. **1945**, 81 (2008).
[7] P. K. Maini, C. R. Biol. **327**, 225 (2004).
[8] G. Sun, Z. Jin, Q. X. Liu, and L. Li, J. Stat. Mech.: Theory Exp. (2007) P11011.
[9] G. Mulone, B. Straughan, and W. Wang, Stud. Appl. Math. **118**, 117 (2007).
[10] R. T. Liu, S. S. Liaw, and P. K. Maini, J. Korean Phys. Soc. **50**, 234 (2007).
[11] Y. Wang, J. Wang, and L. Zhang, Appl. Math. Comput. **217**, 1965 (2010).
[12] N. Kumar, R. R. Parmenter, and V. M. Kenkre, Phys. Rev. E **82**, 011920 (2010).
[13] G.-Q. Sun, Nonlin. Dyn. **69**, 1097 (2012).
[14] V. Mendez, J. Fort, and J. Farjas, Phys. Rev. E **60**, 5231 (1999).
[15] J. Fort and V. Méndez, Rep. Prog. Phys. **65**, 895 (2002).
[16] V. Mendez and J. E. Llebot, Phys. Rev. E **56**, 6557 (1997).
[17] U. I. Cho and B. C. Eu, Physica D **68**, 351 (1993).
[18] A. Lemarchand and B. Nowakowski, J. Chem. Phys. **109**, 7028 (1998).
[19] T. Hillen, Math. Models Methods Appl. Sci. **12**, 1007 (2002).
[20] E. Barbera, C. Curró, and G. Valenti, Appl. Math. Model. **34**, 2192 (2010).
[21] E. Barbera, G. Consolo, and G. Valenti (unpublished).
[22] J. Fort and V. Mendez, Phys. Rev. E **60**, 5894 (1999).
[23] E. Barbera, C. Curró, and G. Valenti, Math. Methods Appl. Sci. **33**, 1504 (2010).
[24] E. Barbera, C. Curró, and G. Valenti, Math. Methods Appl. Sci. **31**, 481 (2008).
[25] S. R. Dumbar and H. G. Othmer, *Nonlinear Oscillations in Biology and Chemistry*, Lecture Notes in Biomathematics Vol. 66 (Springer, Berlin, 1986).
[26] I. Muller and T. Ruggeri, *Rational Extended Thermodynamics* (Springer, New York, 1998).
[27] A. M. Turing, Philos. Trans. R. Soc. London B **237**, 37 (1952).
[28] W. M. Liu, S. A. Levin, and Y. Iwasa, J. Math. Biol. **23**, 187 (1986).
[29] W. M. Liu, H. W. Hethcote, and S. A. Levin, J. Math. Biol. **25**, 359 (1987).
[30] H. W. Hethcote and P. van den Driessche, J. Math. Biol. **29**, 271 (1991).
[31] R. M. Cullen and A. W. J. Korobeinikov, ANZIAM J. **44**, 501 (2003).
[32] A. Korobeinikov and V. Sobolev (unpublished).
[33] B. Buonomo and D. Lacitignola, Ric. Mat. **57**, 261 (2008).
[34] V. Capasso and G. Serio, Math. Biosci. **42**, 43 (1978).
[35] S. Ruan and W. Wang, J. Diff. Eq. **188**, 135 (2003).
[36] A. Korobeinikov and P. K. Maini, Math. Biosci. Eng. **1**, 57 (2004)
[37] A. Korobeinikov and P. K. Maini, Math. Med. Biol. **22**, 113 (2005)
[38] P. Gray and S. K. Scott, Chem. Eng. Sci. **39**, 1087 (1984).
[39] A. Doelman, T. J. Kaper, and P. A. Zegeling, Nonlinearity **10**, 523 (1997).
[40] Y. Nishiuraa and D. Ueyama, Physica D: Nonlin. Phenom. **150**, 137 (2001).
[41] I. S. Liu, Arch. Ration. Mech. Anal. **46**, 131 (1972).
[42] K. O. Friedrichs and P. D. Lax, Proc. Natl. Acad. Sci. USA **68**, 1686 (1971).